Solvated poly-(phenylene vinylene) derivatives: conformational structure and aggregation behavior†‡

Alexander Lukyanov,[ab] Alexander Malafeev,[b] Viktor Ivanov,[b] Hsin-Lung Chen,[c] Kurt Kremer[a] and Denis Andrienko[*a]

We study dilute solutions of poly(2,3-diphenyl phenylene vinylene) with hexyl (DP6-PPV) and decyl (DP10-PPV) side chains in two solvents, chloroform and toluene. For this purpose, atomistic and coarse-grained models are parametrized using quantum-chemical calculations and structure-based coarse-graining, respectively. Our simulations indicate that the difference in the aggregation behavior of two derivatives can not be rationalized just in terms of the greater steric hindrance imposed by the longer side chains of DP10-PPV. The coarse-grained model describes qualitatively the DP10-PPV derivative in chloroform, where aggregation does not occur. Although the computed structure factors for this system qualitatively agree with experiments for low concentrations, the calculated persistence length is bigger than the one experimentally reported, hinting at the presence of defects in polymer chains.

1   Introduction

Conjugated polymers have attracted much interest due to their unique optical and semiconducting properties, making them the materials of choice for opto-electronic applications, e.g. polymer light emitting diodes and plastic conductive layers.[1–3]

Even in the early stages of the design of polymeric optoelectronic devices, it already became clear that the electronic properties of thin films of conjugated polymers are extremely sensitive to the global as well as the local arrangement of chains. By choosing different processing techniques, e.g. spin-coating or drop-casting, and processing conditions, such as solvent and temperature, it is possible to obtain different morphologies and hence control the electronic properties of the film.

The generic molecular architecture of conjugated polymers is comprised of a semi-rigid conjugated backbone, responsible for charge conductance, and flexible side chains that insure solubility and facilitate processing. When drop-casted or spin-coated from solution, the resulting film morphology depends on the chain conformation in dilute solution. Hence, understanding of the conformational structure of conjugated polymers in solutions is necessary in order to control the morphology of a thin organic semiconducting layer.

Experimentally, techniques such as light or neutron scattering are used to study structural properties of polymer solutions. These properties are extracted by fitting scattering profiles to predefined analytical models.[4] However, even an excellent fit

[a]Max Planck Institute for Polymer Research, Mainz, Germany. E-mail: denis.andrienko@mpip-mainz.mpg.de; Fax: +49 6131 379100; Tel: +49 6131 379147
[b]Physics Department, Moscow State University, Moscow, Russia
[c]Department of Chemical Engineering, National Tsing-Hua University, Hsin-Chu, 30013, Taiwan, R.O.C

† This paper is part of a Journal of Materials Chemistry themed issue on Modelling of Materials. Guest editors: Julian Gale and Mark Wilson.
‡ Electronic supplementary information (ESI) available: Further information. See DOI: 10.1039/c0jm01654c

alone can not guarantee that the underlying analytical model is valid. In this situation, computer simulations may be employed to validate the conclusions of experimental studies and help to link morphology and electronic structure to charge or exciton mobility.[5–7] In order to do this, one first has to be able to generate large-scale material morphologies at an atomistic scale resolution. This involves (a) parametrization of atomistic force-fields, since these are not readily available for most organic compounds and (b) development of solvent-free coarse-grained models, capable of back-mapping.[8,9] The latter is essential for extending time- and length-scales accessible to those of classical molecular dynamics simulations.

Here, we illustrate how both of these tasks may be tackled for dilute solutions of conjugated polymers. Specifically, we study two derivatives of poly(2,3-diphenylphenylene vinylene) (DP-PPV) with hexyl (DP6-PPV) and decyl (DP10-PPV) side chains, as shown in Fig. 1a. DP-PPVs have been considered as a family of green-emitting materials for LED applications due to their high glass transition temperature, high fluorescence efficiency, and ease of monomer and polymer synthesis.[10–12] Conformational structure and aggregation behavior of DP6-PPV have been studied by means of small angle neutron scattering (SANS) and
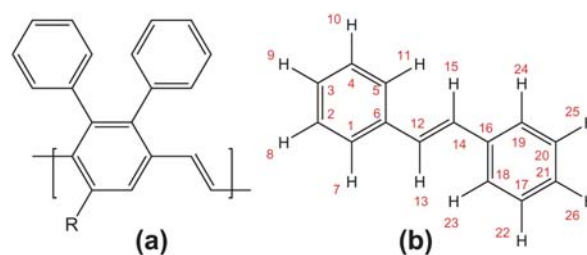

Fig. 1 (a) Chemical structure of DP-PPV derivatives. R = C_6H_{13} corresponds to DP6-PPV and R = $C_{10}H_{21}$ to DP10-PPV. (b) Trans-stilbene - a monomer of poly-(phenylene vinylene) used to validate the re-parametrized atomistic force-field.

dynamic light scattering (DLS).[13] It could be shown that DP6-PPV tends to aggregate in chloroform and toluene, yielding network aggregates whose internal structure can be characterized by a certain fractal dimension. Two types of segmental association with distinct stability were identified for the toluene solution. The highly stable segmental association was attributed to the π–π complex already present in the DP6-PPV powder, while the labile segmental association was ascribed to the poor affinity of the aliphatic side chains of DP6-PPV to toluene. An analogous study for DP10-PPV[14] showed that only a minor fraction of the polymer undergoes segmental association in chloroform, whereas in toluene disk-like clusters are formed. The difference in aggregation behavior between DP6- and DP10-PPV was attributed to the more pronounced steric repulsion of the longer side-chains in the latter polymer.

The paper is organized as follows. First, we re-parametrize and validate the potential energy surface of the atomistic force-field for DP-PPVs using first principles calculations. Then, the results of the atomistic simulations of dilute DP-PPV solutions are presented. Special attention is paid to side-chain stretching, backbone orientational correlations, chain tacticity, and the influence of side groups on the backbone planarity. Subsequently, atomistic trajectories of a single chain in a solvent in combination with the potential of mean force calculations are used to parametrize a coarse-grained model with two repeat units per bead and coarse-grained simulations are performed. These then serve to study large-scale systems and to determine how static structure factors and persistence length change as a function of polymer concentration. We summarize our work by comparing simulation results to experimental data and by commenting on the limitations of our multiscale approach.

All atomistic and coarse-grained molecular dynamics simulations were performed using the GROMACS package,[15,16] while the coarse-graining procedure itself was done with the VOTCA package.[17] First principle calculations were performed with the GAUSSIAN package.[18]

2 Force-field development

As a starting point, we use the OPLS all-atom force-field.[19] Parameters for bonds, angles as well as van der Waals parameters for non-bonded interactions are taken from this force-field. Partial charges and missing bonded interactions are determined using first principles calculations.[20–22] The force-field parametrization is then verified by simulating several thermodynamic properties of trans-stilbene, whose chemical structure is shown in Fig. 1b.

2.1 Partial charges

The CHELPG procedure was used to calculate the partial charges.[23] For geometry optimization we used hybrid DFT functional B3LYP[24] as well as Møller–Plesset second order perturbation theory (MP2). To illustrate the basis set convergence, the charges of the atoms 6 and 12 (see Fig. 1b) are listed in Table 1 as a function of the basis set. One can see that for small basis sets, the variation is about 20%. Saturation is achieved for a rather large basis set, 6-311G++(2d,2p). The DFT values agree well with MP2 calculations, especially for large basis sets. To

Table 1 Partial charges of atoms 6 and 12 as a function of the basis set size. Atom labeling is shown in Fig. 1b

Level of theory	atom No. 6	atom No. 12
B3LYP 6-31G(d,p)	0.227	−0.187
B3LYP 6-311G	0.278	−0.241
B3LYP 6-311G(d)	0.295	−0.248
B3LYP 6-311G(d,p)	0.283	−0.237
B3LYP 6-311+G(d,p)	0.294	−0.243
B3LYP 6-311++G(d,p)	0.301	−0.241
B3LYP 6-311++G(2d,2p)	0.264	−0.216
B3LYP 6-311G(2df,2pd)	0.254	−0.210
MP2 6-31G(d,p)	0.259	−0.222

assess the values of partial charges in a polymer, we have also performed calculations for tetra- and octamers. No significant variations were found. The list of partial charges is available in the Supporting Information.

2.2 Parametrization of backbone dihedrals

To refine the force-field parameters for dihedral angles, we first considered the backbone without the side chains as shown in Fig. 1b. Three dihedral potentials, which are not present in the OPLS force-field, determine the rigidity and conformation of the backbone. To obtain parameters for these potentials, the angle of interest was scanned by optimizing the molecular geometry for a fixed value of the dihedral. The scan provides a set of optimized molecular structures and total energies for each angle value. Subsequently, the energy of each optimized conformation was evaluated with the help of the force-field, where the dihedral of interest was switched off. To do this, the molecular geometry was again optimized for each value of the constrained dihedral angle and the difference between the two energies was fitted, providing the desired dihedral parameters.[25]

For the dihedrals (1-6-12-14) and (6-12-14-16) (see Fig. 1b) the functional form given by eqn (1) was used, while for the improper dihedral (6-1-5-12) the functional form given by eqn (2) was used

$$V = k_\phi[1 + \cos(2\phi - \phi_0)] \tag{1}$$

$$V = \tfrac{1}{2}k_\phi(\phi - \phi_0)^2 \tag{2}$$

where ϕ_0 is the equilibrium angle and k_ϕ is the fitted force constant.

The results of fitting are shown in Fig. 2. For the first dihedral, (1-6-12-14), different levels of theory provide different equilibrium values of the dihedral angle. MP2 calculations suggest that the ground state of trans-stilbene is nonplanar contrary to the DFT calculations. In fact, the discrepancy between these methods is a known issue. A more detailed study of trans-stilbene shows that it is planar and the value of the torsional barrier is 14.3 kJ/mol.[26] This value was used for fitting. The results for all three dihedrals are summarized in Table 2.

2.3 Force-field validation

To validate the force-field, we compared the dimensions of the simulated and experimentally measured unit cell of trans-stilbene crystal and its melting temperature.
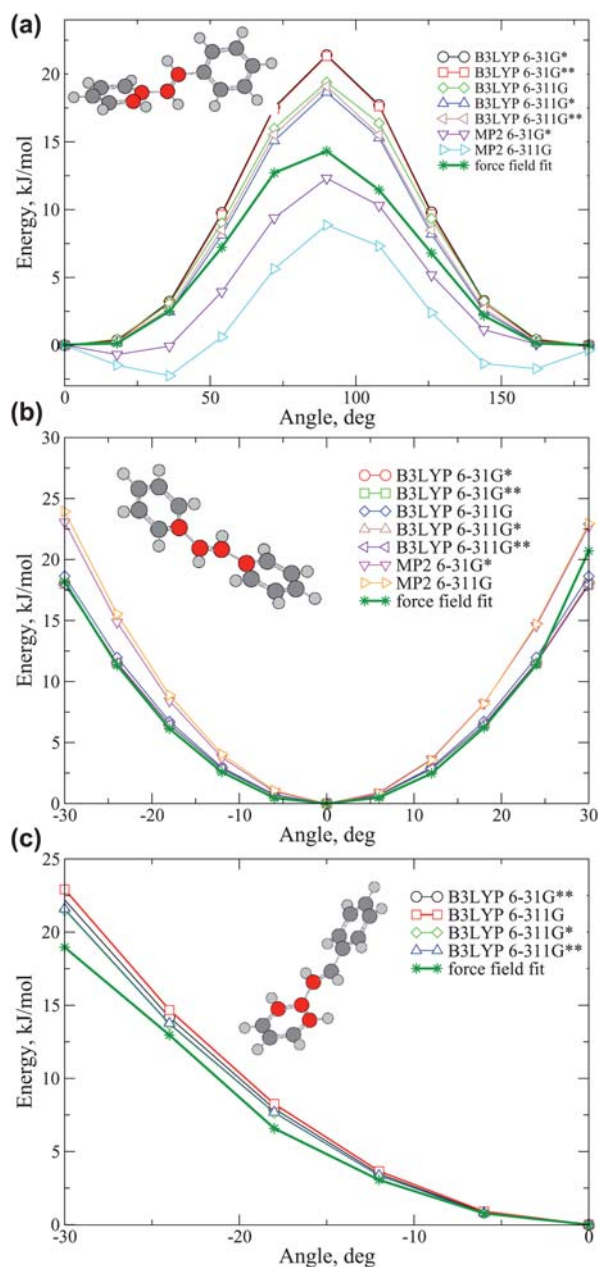
Fig. 2 Energies calculated using first principle methods as well as fitted force-field potentials for the dihedrals: (a) 1-6-12-14 (b) 6-12-14-16 (c) 6-1-5-12. The scanned dihedrals are depicted in the insets. Different methods and basis sets are shown.

Table 2 Dihedral parameters. See Fig. 1b and Fig. 2 for notations

dihedral	ϕ_0, deg	k_ϕ, kJ/mol
1-6-12-14	0	7
6-12-14-16	0	30
6-1-5-12	0	270

The monoclinic unit cell of trans-stilbene[27] was multiplied as $2a \times 4b \times 2c$ to be able to use 0.9Å cutoff distance for Van der Waals interactions. After energy minimization with the conjugate gradient method,[28] a 200 ps molecular dynamics run in the

Table 3 Monoclinic unit cell parameters of trans-stilbene. All distances are given in Å

	Experiment[27]	MD simulations
a	12.287 ± 0.003	12.09 ± 0.06
b	5.660 ± 0.003	5.38 ± 0.06
c	15.478 ± 0.005	16.9 ± 0.2
β, deg	112.03 ± 0.1	110.0 ± 0.2

NPT ensemble (anisotropic Berendsen thermostat,[29] $P = 1$ bar, $T = -160$ °C) was performed. After equilibration, an NPT production run of 600 ps was performed. The simulated density of trans-stilbene was 1161 kg/m³, which is in a good agreement with the experimental value of 1200 kg/m³ as well as the crystallographic parameters given in Table 3.

To simulate the crystal melting, we performed a simulated annealing run, increasing the temperature from -160 °C to 180 °C during 1200 ps (heating rate 0.283 °C/ps). While monitoring the mean squared displacement and density of the compound, as shown in Fig. 3. We concluded the melting point to be 127 ± 25 °C. To reduce the error bars, a set of 200 ps NPT simulations at 102 °C, 112 °C, 122 °C, and 132 °C were performed. Up to 122 °C, the system remains in the crystalline state, melting completely at 132 °C. Our predicted melting point of 127 ± 5 °C agrees well with the experimental value of 124 ± 1 °C. To ensure that the system size and the heating rate do not affect
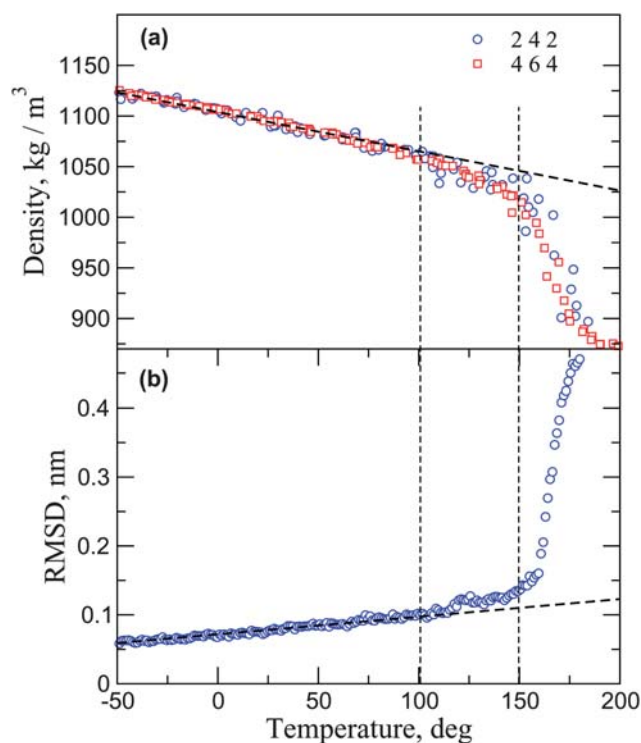

Fig. 3 (a) Density as a function of temperature during a 1200 ps simulated annealing run. Two system sizes are shown: $2a \times 4b \times 2c$ and $4a \times 6b \times 4c$. The results suggest that the melting point of trans-stilbene is 127 ± 25 °C. (b) Root mean square deviation from the equilibrium crystalline structure as a function of temperature. 1200 ps simulated annealing. Melting occurs at 1020 ± 80 ps, which corresponds to 127 ± 25 °C.

This journal is © The Royal Society of Chemistry 2010

J. Mater. Chem., 2010, **20**, 10475–10485 | 10477

the results, we also annealed a $4a \times 6b \times 4c$ cell. The results are shown in Fig. 3, indicating that there are no significant finite size effects. Within the range of 0.07–0.3 deg/ps, we did not observe any dependence on the heating rate.

In summary, we can conclude that the performance of our force-field for trans-stilbene is adequate.

2.4 DP-PPV force-field

To derive the force-field for DP6-PPV and DP10-PPV, we followed the same strategy. We first calculated the partial charges of a DP-PPV monomer unit and then parametrized two additional dihedral potentials. The first one, linking phenyl rings to the backbone and the second one, connecting the backbone phenyl ring and the alkyl side chain. The Ryckaert-Belleman functional form[30] was used to parametrize these two dihedrals

$$V_{rb}(\phi) = \sum_{n=0}^{5} C_n \cos^n \phi \qquad (3)$$

where $\phi = 0$ corresponds to the trans-conformation. The obtained constants, C_n, are given in Table 4. For the alkyl side chains, we used the OPLS united atom force-field.[19] The force-field files (in GROMACS format) are available in the Supporting Information.

2.5 Solvents

A four-site model was used for chloroform. In this representation, one molecule consists of 3 chlorine atoms (Cl) and one united atom (CH). Corresponding Lennard-Jones parameters and partial charges are given in Table 5. The bonded parameters for the CH–Cl bond were $b_0 = 0.17580$ nm, $k_b = 459403.2$ kJ mol^{-1} nm^{-2}. For the Cl–CH–Cl angle: $\theta_0 = 111$ deg, $k_\theta = 600$ kJ mol^{-1} rad^{-2}. For toluene, the CH$_3$ group was combined in a united atom, while the rest of the atoms were treated explicitly.[31,32]

To test the force-field performance for solvents, we equilibrated 125 chloroform molecules for 2 ns in an NPT ensemble at temperature 300 K and pressure 1 bar. The equilibrium density of 1.45 ± 0.01 g/cm^3 was in excellent agreement with the experimental value of 1.48 g/cm^3. The calculated diffusion coefficient of $D = (2.94 \pm 0.01) \times 10^{-5}$ cm^2/s was also in a reasonable agreement with the experimental value of 2.32×10^{-5} cm^2/s.[33]

For toluene, both the simulated density of 0.869 ± 0.004 g/cm^3 and the diffusion constant of $(2.2 \pm 0.1) \times 10^{-5}$ cm^2/s agreed well with the experimentally measured values of 0.87 g/cm^3 and 2.1×10^{-5} cm^2/s respectively.[34]

Table 4 Ryckaert-Belleman parameters for (i) the dihedral linking two phenyl rings and (ii) the dihedral connecting the backbone phenyl ring with the alkyl side chain. All constants are in kJ/mol

	C_0	C_1	C_2	C_3	C_4	C_5
(i)	8.60	0.0	−30.81	0.0	21.66	0.0
(ii)	−4.22	−0.027	9.44	0.48	−5.15	−0.47

Table 5 Non-bonded force-field parameters for chloroform

Atom	σ, nm	ε, kJ/mol	charge, e
CH	0.38	0.326944	0.420
Cl	0.347	1.25604	−0.140

3 Atomistic molecular dynamics

In this section, we present results of our atomistic molecular dynamics simulations such as side chain stretching, planarity of the backbone, and chain persistence length in two solvents. Throughout the text, we use the following abbreviations for different polymer derivatives, solvents, and backbone lengths: each system name begins either with D6 or D10, corresponding to DP6-PPV or DP10-PPV respectively. An additional letter denotes the solvent: "c" is for chloroform and "t" for toluene. Finally, a number for the backbone chain length, in repeat units, is added. For example, D6c20 is a 20 monomer units long DP6-PPV derivative in chloroform. Unless otherwise stated, all simulations were performed at 300 K.

3.1 Alkyl side chain stretching in solvated DP-PPV

Experimentally, chloroform is considered to be a relatively good solvent for both DP6- and DP10-PPV derivatives, whereas toluene is a relatively poor one. Additional segmental aggregation in toluene relative to chloroform is often ascribed to the poor affinity of the aliphatic side chains of DP-PPV for toluene.[13,14] To check this, we analyzed alkyl side chain stretching in both solvents.

A 10-mer of DP6- or DP10-PPV was simulated in chloroform and toluene for 40 ns and the corresponding distributions of the side chain end-to-end distances are shown in Fig. 4. As one can see, the distributions are identical for both solvents, *i.e.* the difference in solvent quality does not affect the side chain conformations, at least in our atomistic model. The same conclusion could be made when simulating an all-atom hexane chain (which corresponds to a side chain of DP6-PPV) in chloroform and toluene, where again, no effect of solvent quality on chain conformations was detected.

Experimentally, solvent quality can be characterized *via* the second virial coefficient A_2, which can be determined from static light scattering experiments.[14] $A_2 = 6.7 \times 10^{-6}$ mol dm^3 g^{-2} was reported for chloroform and 3.7×10^{-6} mol dm^3 g^{-2} for toluene. This difference is rather small and poses the question of whether toluene is a poorer solvent than chloroform only because of the additional chain aggregation observed in toluene solutions.[13,14] It is also interesting that toluene is often reported to be a good solvent for another PPV derivative, MEH-PPV,[35] as well as for polyfluorenes with longer alkyl side chains.[36,37] This further suggests that both toluene and chloroform might be relatively good solvents for DP-PPVs and that aggregation is an artifact of an initial non-equilibrium state of polymer chains in a powder.

3.2 Orientational correlations in solvated DP-PPV

Orientational correlations of the polymer backbone can be used to calculate the persistence length of a chain, which can be directly compared to experimental values.
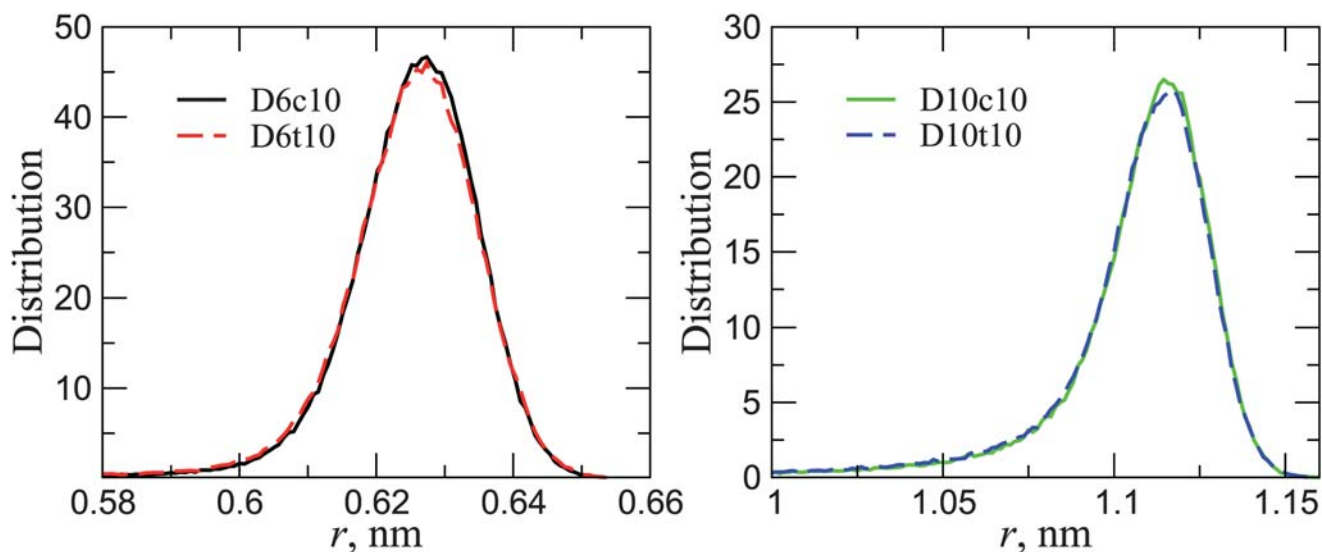
Fig. 4 Alkyl side chain end-to-end distance distributions for DP6- and DP10-PPV chains of 10 repeat units. Chain stretching does not depend on the solvent. Name abbreviations are explained in sec. 3.

A single chain of 20 monomer units was solvated in previously equilibrated solvent boxes, containing 23550 and 17728 molecules of chloroform and toluene respectively. After 10 ns of equilibration, a production run of 40 ns was performed. During the production run, the orientational correlations of repeat units were calculated as

$$\cos\theta_n = \langle e_i \cdot e_{i+n} \rangle \qquad (4)$$

where e_i is a unit vector giving the orientation of the i-th repeat unit along the backbone. This orientation is defined by a pair of carbon atoms for a backbone benzene ring, such as atoms 3 and 6 or 16 and 21 in Fig. 1b. $\langle \dots \rangle$ denotes the time average and the average over all pairs, i, $i + n$, along the chain. The persistence length, l_p, can be estimated as $\log(\cos\theta_n) \propto -nl/l_p$, where l is the length of the repeat unit. Note, that this is only possible if correlations decay exponentially, which might not necessarily be the case.[38–40]

Orientational correlations for different solvents and different side-chain lengths are shown in Fig. 5a. It is clear that the backbone is quite rigid (see also Fig. 5d, where a typical conformation of a DP10-PPV chain in chloroform is shown). Moreover, within available accuracy, the decay of the correlation function does not depend on the side-chain length or solvent. A fit yields a rough estimate of the persistence length, $l_p \sim 17$–25 Å. Improved statistical averages are needed for more accurate estimates of l_p, which can be obtained by using solvent-free coarse-grained models, as described in sec. 4.

3.3 Planarity and tacticity of solvated DP-PPV

To facilitate charge transport along a conjugated chain, planarity of the backbone is required.[41] In principle, conjugation already enforces a planar backbone conformation. However, non-bonded (Coulomb and van der Waals) contributions can favor twists in the backbone. Here, we study how the chemical structure of a repeat unit, in particular the side chain groups, affects the planarity and tacticity of the backbone.

A PPV repeat unit has two dihedral angles which control its planarity, as depicted in the inset of Fig. 6a. Fig. 2a shows the dihedral potential of trans-stilbene, corresponding to these angles. It has two minima separated by a barrier significantly higher than $k_B T$. Since both minima are rather shallow, thermal fluctuations can easily lead to a 45 degree twist in the backbone, breaking the conjugation.

To study the effect of varying side chains on the dihedral distributions, we simulated three model systems, all based on a DP6-PPV trimer. The first one, referred to as a "bare backbone" system, had both alkyl side chains and phenyl rings (not belonging to the backbone) substituted with hydrogens. The second system did not have aliphatic side chains, while the last system had the non-bonded interactions of the phenyl rings not belonging to the backbone switched off.

The distributions of the dihedral angles for these three cases are shown in Fig. 6. The distributions for a backbone without any side groups, Fig. 6a, are rather broad with the maxima located at 0 and $\pm$ 180 deg. Due to the symmetry of the "bare backbone" PPV, both distributions are identical and probabilities of finding the system with angles of 0 deg and $\pm$ 180 deg are the same. The distributions became asymmetric for the systems with the alkyl side chains, as shown in Fig. 6c. Here, one of the dihedral angles samples conformations around 0 deg and the other those of around 180 deg. This reflects the fact that the alkyl side chains repel each other and are attached in an asymmetric way with respect to the two dihedrals. Hence, the symmetry of the distributions with respect to the angles is broken. If instead, only the phenyl rings are attached, the cis conformation becomes improbable, as can be seen in Fig. 6b. In this case, the $\phi = 0$ deg conformation is more preferable than the $\phi = \pm$ 180 deg one. Both effects add up in the distributions of DP6-PPV, which are shown in Fig. 6d. Here, the heights of the distributions of the dihedral angles ϕ_1 and ϕ_2 are different at $\phi = 0$ deg, which is due to alkyl side chains. Additionally, conformations with $\phi = \pm$ 180 deg are
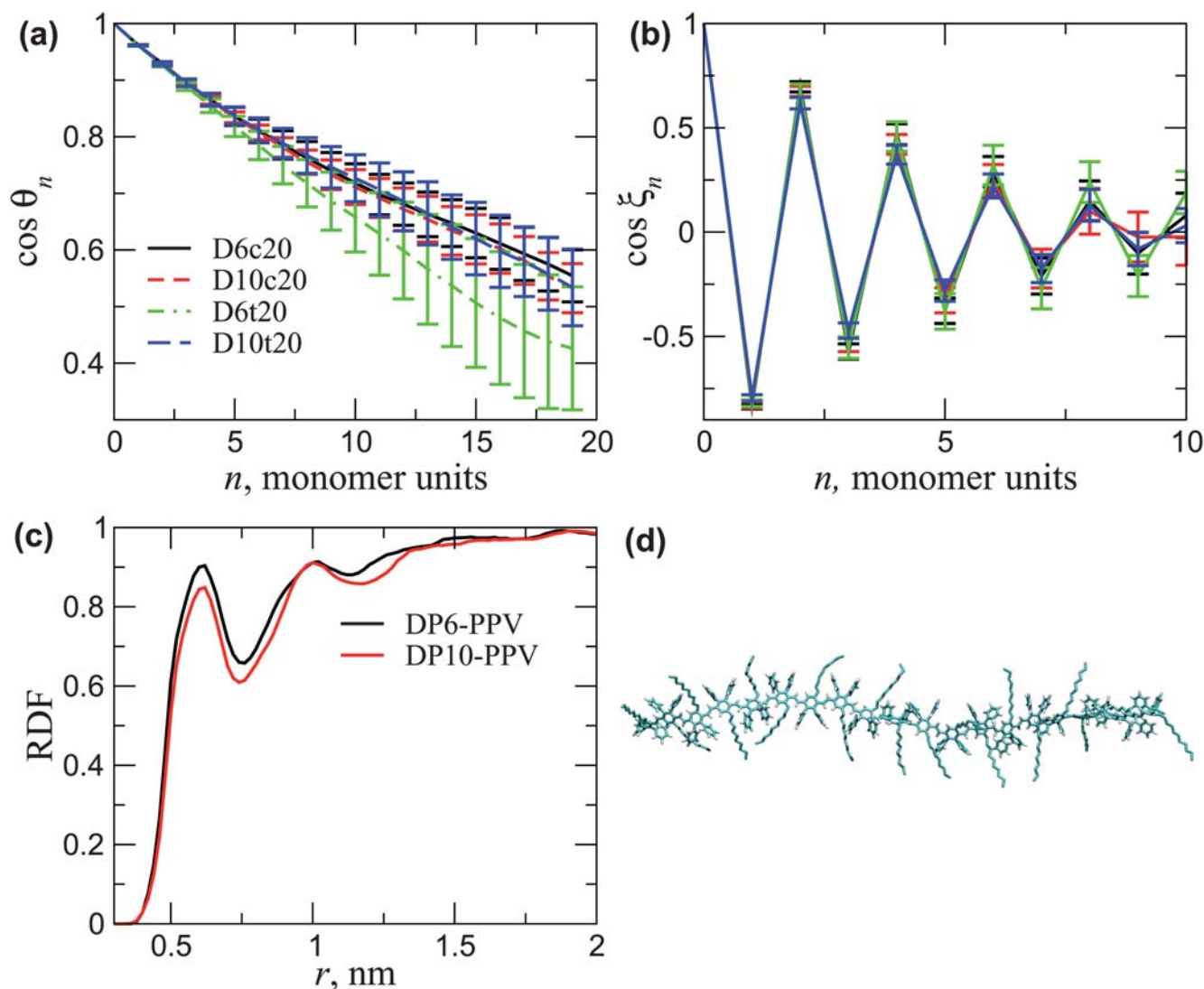
Fig. 5 (a) Orientational correlations for 20 repeat unit chains of DP6- and DP10-PPV in chloroform and toluene. 40 ns run, average of 20000 configurations. (b) Orientational correlations of neighboring monomer units. Correlation functions show that DP-PPV polymers are syndiotactic. (c) Intermolecular radial distribution function for phenyl rings in the melt of DP-PPV oligomers. (d) Typical conformation of a DP10-PPV chain in chloroform.

strongly suppressed due to the presence of the phenyl rings. For the DP10-PPV derivative, the situation is qualitatively similar. Namely, longer alkyl side chains lead to an even broader distribution of the dihedral angle ϕ_2.

The final issue we would like to address here is the tacticity of a DP-PPV polymer chain. It is important for choosing an appropriate mapping for a coarse-grained model, as discussed in sec. 4. By analyzing the distributions of the backbone dihedral angles, we have concluded that the presence of the phenyl side groups leads to chain conformations with opposite orientations of alkyl side chains of neighboring repeat units, *i.e.* DP-PPV is a syndiotactic polymer. In order to see the effect of solvent and side chain length on correlations of monomer orientations, we calculated the correlation function of a cross product of vectors connecting the atoms 2–4 and 18–19 (see Fig. 1b for atom designations). This cross-product, which is a measure of a chain deviation from planarity, is shown in Fig. 5b. Again, within

available accuracy, our model cannot differentiate between toluene and chloroform or hexyl and decyl side chains.

3.4 DP-PPV melt

An interesting observation made on the basis of WAXS experiments is that, in a powder, DP6-PPV forms a π–π complex but DP10-PPV does not.[13] This conclusion was made by analyzing WAXS profiles, which have a sharp maximum at 3 Å in the case of DP6-PPV, and ascribed to the distance between the π-stacked phenyl rings. This maximum was absent in the DP10-PPV powder. The difference in ring packing was explained in terms of the bulkier side chains of DP10-PPV as compared to those of DP6-PPV.

To capture the influence of the alkyl side chain length on packing, we simulated a melt of DP-PPV oligomers. 64 oligomers of 5 monomer units each were assembled on a regular lattice with
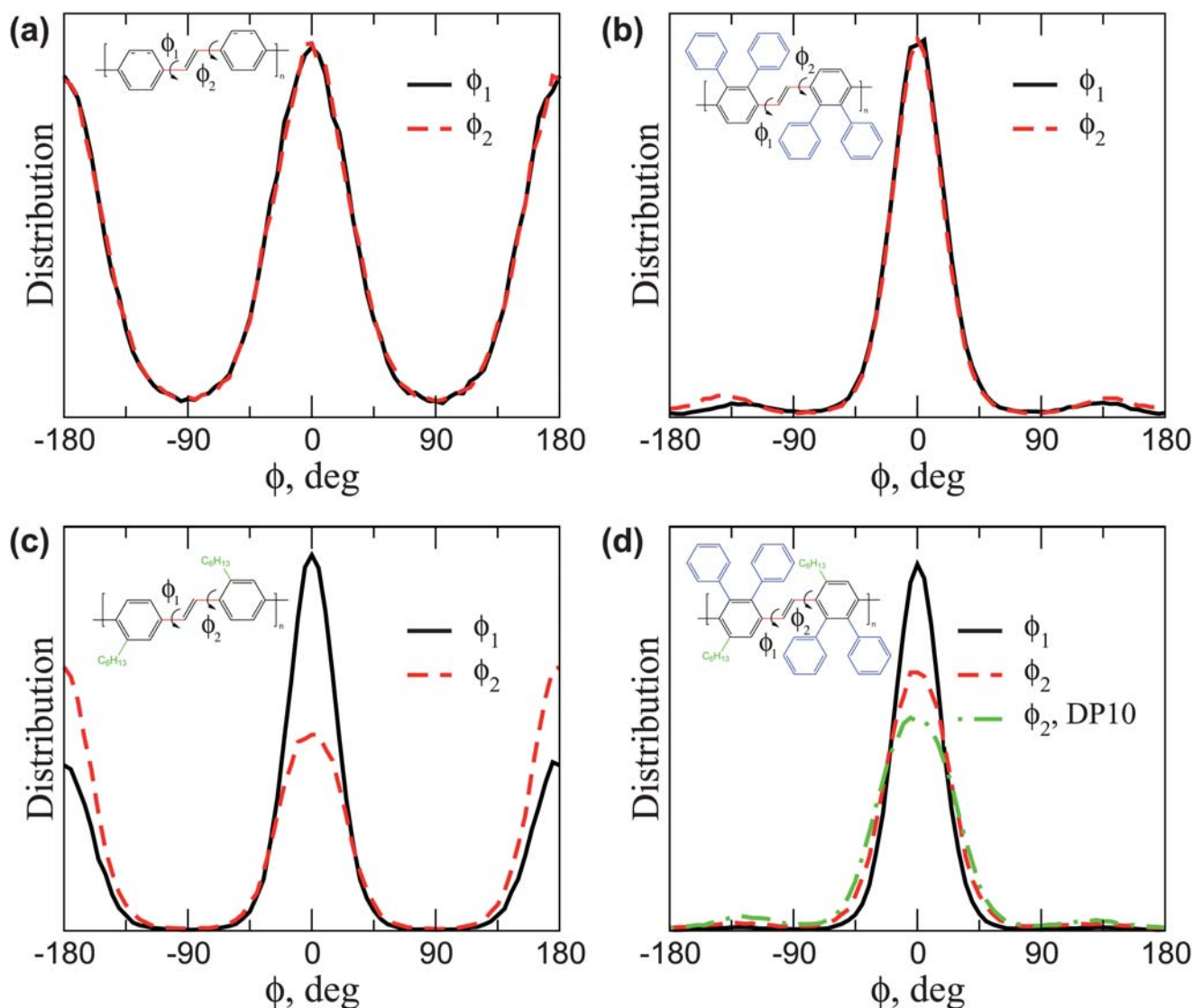
Fig. 6 Distributions of dihedral angles controlling planarity of the PPV unit. (a) Bare PPV, without the side chains and phenyl rings. (b) Phenyl rings only. (c) Side chains only. (d) DP6-PPV. All results stem from a single chain in vacuum. Insets depict the chemical structure of the corresponding compounds.

low density. NPT simulations were performed to compress the system, which was then heated to 700 K, equilibrated for 20 ns, and cooled down to 300 K.

The radial distribution function of the centers of mass of the phenyl rings is shown in Fig. 5c. As one can see, it is practically identical for the melts of DP6- and DP10 oligomers. Hence, in a melt of oligomers, the average distance between phenyl rings is not sensitive to the length of side chains. Of course, the melt morphology might differ from the non-equilibrium semi-crystalline morphology of a polymer powder. Nevertheless, some π–π complexes should also appear in the melt and their amount and the π–π distance should depend on the length of the side chains. Since this is not the case, atomistic models hint that the absence of π–π complexes in DP10-PPV powder is due to the non-equilibrium state of the polymer.

Another interesting experimental observation is the crystallization of polymer backbones upon annealing of a spin-coated

film. Crystallization leads to a significantly more pronounced X-ray diffraction peak at a π–π stacking distance, which is reported to be 3 Å.[3] Fig. 5c indeed shows that after annealing, the first maximum of the radial distribution function is located at a separation of about 6 Å. In fact, this separation corresponds to the minimum of the potential of mean force of two coarse-grained beads in vacuum as shown in Fig. 7c. It obviously overestimates the π–π staking distance since the system is in a non-equilibrium state. However, the reported in experiments separation of 3 Å is too small and already in the range of the repulsion of two cofacially aligned repeat units, even without any side chains attached to them.[42]

3.5 Atomistic molecular dynamics: summary

In summary, the all-atom molecular dynamics simulations give similar and often identical results for DP6-PPV and DP10-PPV
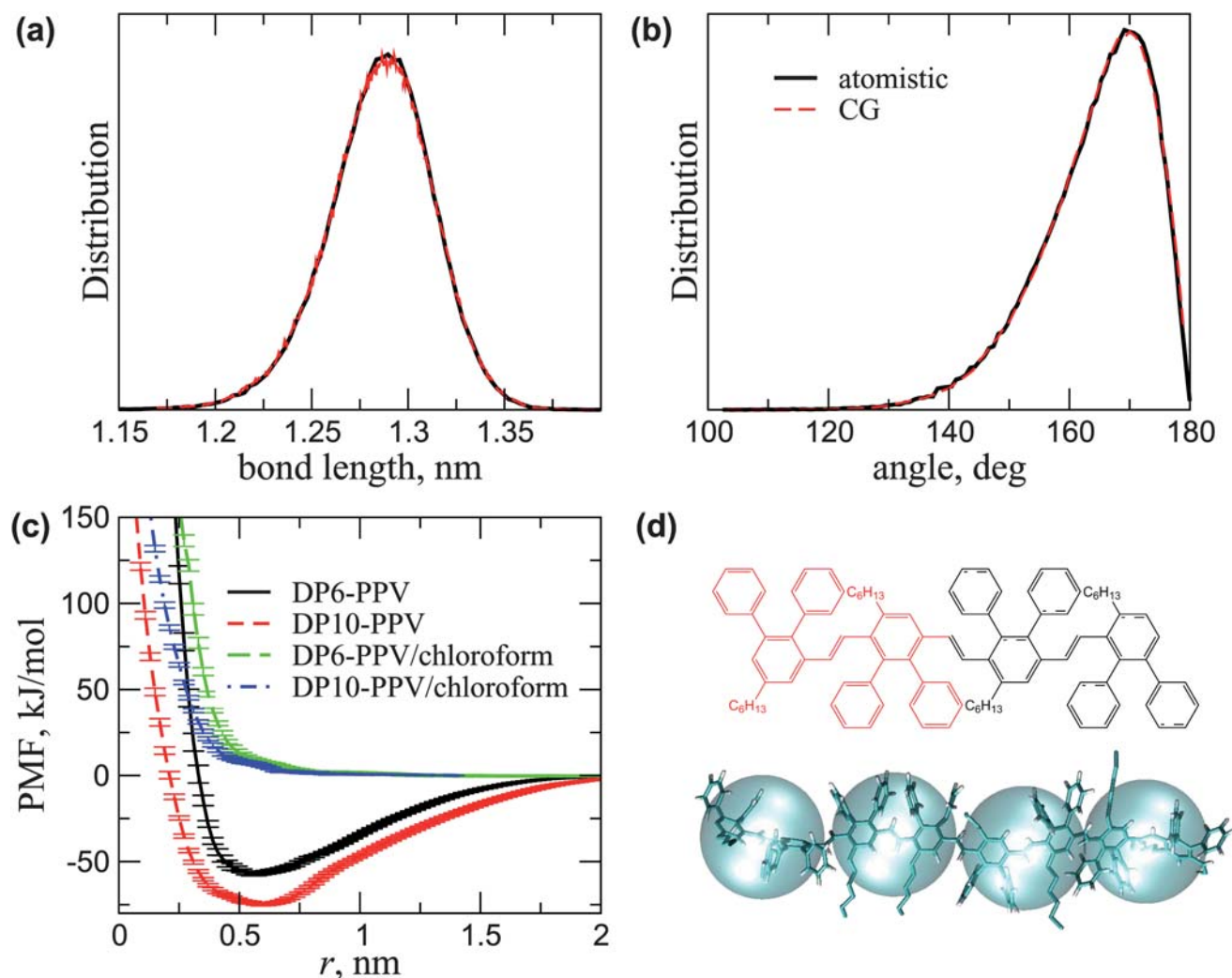
Fig. 7 (a) Bond and (b) angle distribution functions as obtained from atomistic and coarse-grained MD simulations. A chain of 20 monomers of DP10-PPV in chloroform was used for sampling. Potentials are obtained by Boltzmann-inverting the distributions. (c) Dimer-dimer potential of mean force (PMF), calculated using configurational sampling. PMFs in toluene are identical to those in chloroform. (d) Mapping scheme for the coarse-grained model. When determining centers of coarse-grained beads, no alkyl side chains were included.

in both solvents, *i.e.* we could not capture the difference in solvent quality. Longer side chains of DP10-PPV as compared to DP6-PPV do neither affect phenyl ring packing in a melt nor dimer-dimer interactions in vacuum and solution, as will be shown in sec. 4.3. Hence, experimentally observed fractal aggregates of DP6-PPV in chloroform or disk-like aggregates of DP10-PPV in toluene, can not be rationalized by atomistic models. However, reasonable agreement with experiments can be expected for a dilute solution of DP10-PPV in chloroform, since in this case no aggregation occurs. In the following section, we will develop a solvent-free coarse-grained model of DP10-PPV in chloroform.

4 Coarse-grained model

Coarse-graining is a systematic way of reducing the number of degrees of freedom when representing a system of interest. Coarse-grained models are computationally more efficient than atomistic ones and are widely used to study phenomena which

occur on time- or length-scales not accessible to atomistic simulations.[8,43–48]

As has already been pointed out in sec. 3, atomistic simulations do not allow an accurate estimation of polymer persistence lengths. Moreover, for studying dilute solutions of DP-PPV in chloroform or toluene, systems with many chains have to be simulated at different concentrations, which is practically impossible at the atomistic level of detail.

In this section, we develop a solvent-free coarse-grained model for DP10-PPV in chloroform and use it to calculate persistence length and static structure factor as a function of polymer concentration. Both are then compared to the experiment.

4.1 Mapping scheme

To represent a DP-PPV chain on a coarse-grained level, we mapped two monomer units onto one spherical bead, as illustrated in Fig. 7d. Two (instead of one) monomer units per bead were used because PPV is syndiotactic, as discussed in sec. 3.3. Hence, a coarse-grained representation with one bead per repeat

unit is problematic, since repeat units are asymmetric and cannot be properly described by spherically-symmetric pair potentials.

4.2 Bonded interaction potentials

The next step of systematic coarse-graining is to determine bonded and non-bonded potentials. Here, we decided to have only two types of bonded interactions, namely a bond stretching potential between two successive beads and an angle potential between three successive beads. Dihedral potentials are not included as DP-PPVs have a rigid backbone which can be accounted for by the angular potential only. To parametrize the bonded potential, we followed an approach in which bonded interactions are obtained from canonical sampling of a single chain in a solvent. The potentials are then obtain by Boltzmann inverting the corresponding distribution functions,[43] as implemented in the VOTCA package.[17] Specifically, a single chain of 20 repeat units of DP10-PPV in chloroform was used. Resulting distributions for both atomistic and coarse-grained sampling are in perfect agreement with each other as shown in Fig. 7a,b.

4.3 Non-bonded interaction potentials

For non-bonded coarse-grained interaction potentials we used the potential of mean force (PMF) between dimers. In this case, PMF is a free energy of a dimer pair at a specific separation, averaged over all possible mutual orientations of the dimers, as well as positions and orientations of solvent molecules, if present. Note that non-bonded potentials are often obtained by Boltzmann inverting, sometimes iteratively, of radial distribution functions (RDFs). It is practically impossible to obtain accurate RDFs for a dilute solution due to the presence of the explicit solvent. Hence, to simulate dilute solutions, we used PMF in a solvent as a non-bonded potential.

PMFs for both DP6- and DP10-PPV were calculated in vacuum and solvents, using configurational sampling.[49] Results

are shown in Fig. 7c. In vacuum, PMF predicts strong dimer-dimer attraction, which might lead to polymer aggregation. On the other hand, fully solvated dimers have a purely repulsive interaction. Calculated PMFs, and hence the coarse-grained non-bonded potentials, correspond to infinitely dilute systems. In practice, potentials might depend on polymer concentration. However, for systems of up to 1 wt% this dependence may be neglected. In addition, PMFs in both solvents are purely repulsive and only ensure that coarse-grained beads have a certain excluded volume. Hence, simulation results should not be sensitive to the actual functional form of the potential.

4.4 Coarse-grained simulations of DP10-PPV in chloroform

Experimentally, three different concentrations of DP10-PPV/ chloroform solutions were studied: 0.1, 0.5, and 1.0 wt%.[14] We used the same concentrations as in experiment and compared simulated and measured polymer persistence lengths and static structure factors.

The systems consisted of 512 polymer chains, 50 beads each, which corresponds to 100 monomer units. NVT simulations were performed for 16 ns and 800 frames were used to compute static structure factors. All coarse-grained simulations were performed at 300 K.

The calculated structure factors, $S(q)$, for different polymer concentrations are shown in Fig. 8a. One can see that $S(q)$ scales as q^{-1} in the high-q region, irrespective of concentration. This is due to the rod-like nature of the segments constituting the DP10-PPV chains.[50] In the low-q region, intensity decreases with an increase of concentration. This dependence is determined by the dynamic network structure formed by the interchain overlap in the semidilute solution.[51]

Backbone orientational correlations are shown in Fig. 8b. These correlations decay exponentially on the accessible length scale, which allows estimations of polymer persistence lengths as
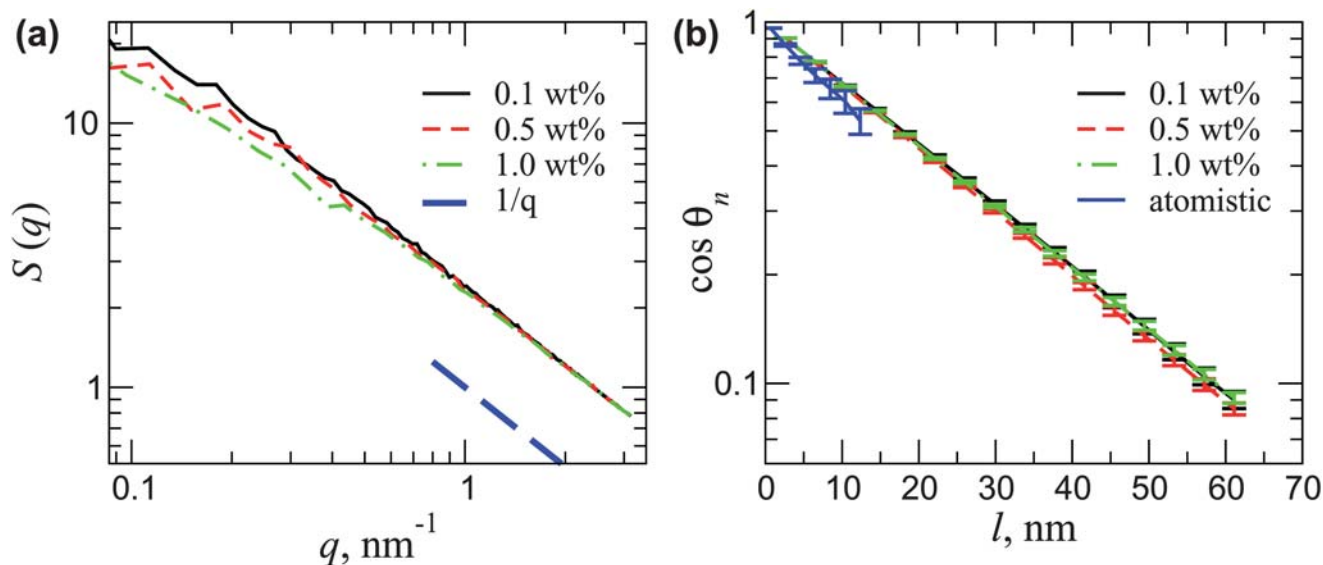

Fig. 8 (a) Calculated static structure factors for DP10-PPV solutions for different polymer concentrations. All systems contain 512 chains of 50 beads each. We vary the polymer concentration by changing the size of the simulations box. (b) Backbone orientational correlations for DP10-PPV/chloroform solutions for different concentrations. Results from atomistic simulations, Fig. 5a, are shown for comparison.

discussed in sec. 3.2. The calculated persistence length of 25 ± 0.5 nm is independent of concentration, contrary to experimental findings summarized in Table. 6. In experiments, persistence length was extracted by fitting SANS profiles to the wormlike chain model with excluded-volume interactions.[14]

The increase with concentration can be attributed to chain aggregation. At low concentrations, chains do not interact and there is no aggregation. Upon increasing the concentration, aggregates start to form and inside those aggregates, chains become locally more extended which increases their persistence length. Our model can not capture this effect since we have repulsive effective potentials. Hence, no driving force is present, which might lead to polymer aggregation at higher concentrations.

5 Discussion and conclusions

In conclusion, a force-field for DP-PPV derivatives was parameterized and used to study side chain stretching, backbone orientational correlations, tacticity, and planarity as well as the influence of the side chain length on packing of backbones in a melt. Atomistic simulations were also used to calculate polymer-polymer solvent-mediated interaction potentials from which solvent quality was estimated. Finally, a coarse-grained model with two repeat units per bead was parameterized and used to study the persistence length and static structure factor of dilute solutions of poly(2,3-diphenyl phenylene vinylene) in chloroform and toluene.

Our simulations confirm experimental evidence that both chloroform and toluene are good solvents for DP-PPVs. This is based on alkyl side chain stretching, backbone orientational correlations, and the potential of mean force (PMF) of DP-PPV dimers in the solvent. However, the experimentally reported quantitative results on solvent quality could not be reproduced.

Atomistic simulations show that the difference in side chain lengths of DP6- and DP10-PPV does not affect chain packing in a melt of oligomers, which is practically identical for both DP6- and DP10-PPV. Interdimer interactions in solutions are also not strongly affected by the difference in side chain lengths, namely the interdimer PMF is repulsive for both DP6- and DP10-PPV. This seems to contradict experimental observations which find that DP6-PPV forms aggregates in solution, whereas DP10-PPV does not. A possible reason for this inconsistency might be that in experiments, the system is in its non-equilibrium state, since powder, in which polymer chains are semicrystalline, was used to prepare the solution. Furthermore, as can be found in Ref. 14, DP10-PPV does aggregate in toluene solutions. However, if the system is heated up to 85 °C and then cooled down, these

aggregates tend to disappear. Recently, an alternative explanation of anomalous aggregation in good polymer solutions has been proposed.[52] This mechanism is applicable to stereoregular polymers, such as DP-PPV, which indeed shown to be syndiotactic in our simulations.

Coarse-grained simulations show that, for very low polymer concentrations (0.1–1.0 wt%), polymer persistence length does not depend on polymer concentration. This again contradicts the experimental picture, where the increase of persistence length at 1.0 wt% is rationalized as chain aggregation. The overestimation of the polymer persistence length in simulations might be due to the presence of tetrahedral chemical defects in real samples.[53] In these defects conjugated carbon-carbon bonds are replaced by tetrahedral ones. They divide polymer chains into structurally identifiable quasi-straight segments and reduce orientational correlations, which leads to a decrease in persistence length.

Finally, we should mention that various approximations in our simulation models might also lead to a disagreement between experiments and simulations. For example, as experimental data for conjugated compounds is rather sparse, force-field validation becomes problematic. To this end, although we have reproduced density, melting temperature, and crystal structure of stilbene, this is no guaranty that thermodynamic properties such as solvation free energy are correctly reproduced. Other issue can be limited accessible length- and time-scales. Explicit solvents and rather stiff polymer backbones prohibit the study of global chain conformations and chain self-interactions via atomistic molecular dynamics. Solvent-free coarse-grained models are capable of simulating bigger boxes on longer timescales. These, however, lead to additional approximations, which cannot be easily controlled.

Acknowledgements

References

1 J. H. Burroughes, D. D. C. Bradly, A. R. Brown, R. N. Marks, K. Mackay, R. H. Friend, P. L. Burns and A. B. Holmes, *Nature*, 1990, **347**, 539.
2 R. H. Friend, R. W. Gymer, A. B. Holmes, J. H. Burroughes, R. N. Marks, C. Taliani, D. D. C. Bradley, D. A. dos Santos, J. L. Bredas, M. Löglund and W. R. Salaneck, *Nature*, 1999, **397**, 121.
3 H. Spreitzer, H. Becker, E. Kluge, W. Kreuder, H. Schenk, R. Demandt and H. Schoo, *Adv. Mater.*, 1998, **10**, 1340.
4 J. Pedersen and P. Schurtenberger, *Macromolecules*, 1996, **29**, 7602–7612.
5 J. Kirkpatrick, V. Marcon, J. Nelson, K. Kremer and D. Andrienko, *Phys. Rev. Lett.*, 2007, **98**, 227402.
6 J. Kirkpatrick, V. Marcon, K. Kremer, J. Nelson and D. Andrienko, *J. Chem. Phys.*, 2008, **129**, 094506.

Table 6 Estimations of persistence length from SANS experiments[14] and coarse-grained MD simulations. MD predicts the same value for all three concentrations

concentration, wt%	l_p, nm
0.1	6.4
0.5	13.3
1.0	23.0
MD	25.0 ± 0.5

7 X. Feng, V. Marcon, W. Pisula, M. Hansen, J. Kirkpatrick, F. Grozema, D. Andrienko, K. Kremer and K. Müllen, *Nat. Mater.*, 2009, **8**, 421–426.

8 W. Tschöp, K. Kremer, O. Hahn, J. Batoulis and T. Burger, *Acta Polym.*, 1998, **49**, 75–79.

9 C. Peter and K. Kremer, *Soft Matter*, 2009, **5**, 4357.

10 B. Hsieh, H. Antoniadis, D. Bland and W. Feld, *Adv. Mater.*, 1995, **7**, 36.

11 B. Hsieh, Y. Yu, E. Forsythe, G. Schaaf and W. Feld, *J. Am. Chem. Soc.*, 1998, **120**, 231.

12 W. Wan, H. Antoniadis, V. Choong, H. Razafitrimo, Y. Gao, W. Feld and B. Hsieh, *Macromolecules*, 1997, **30**, 6567.

13 Y. C. Li, K. B. Chen, H. L. Chen, C. S. Hsu, C. S. Tsao, J. H. Chen and S. A. Chen, *Langmuir*, 2006, **22**, 11009.

14 Y.-C. Li, C.-Y. Chen, Y.-X. Chang, P.-Y. Chuang, C. J-H, H.-L. Chen, C.-S. Hsu, V. Ivanov, P. Khalatur and S.-A. Chen, *Langmuir*, 2009, **25**, 4668–4677.

15 E. Lindhal, B. Hess and D. van der Spoel, *J. Mol. Model.*, 2001, **7**, 306.

16 B. Hess, C. Kutzner, D. van der Spoel and E. Lindahl, *J. Chem. Theory Comput.*, 2008, **4**, 435.

17 V. Rühle, C. Junghans, A. Lukyanov, K. Kremer and D. Andrienko, *J. Chem. Theory Comput.*, 2009, **5**, 3211.

18 M. Frisch et al., *Gaussian 03, Revision B.03*, Gaussian Inc., Wallington CT, 2004.

19 W. L. Jorgensen and J. Tirado-Rives, *J. Am. Chem. Soc.*, 1988, **110**, 1657.

20 A. Lukyanov, C. Lennartz and D. Andrienko, *Phys. Status Solidi A*, 2009, **206**, 2737–2742.

21 V. Rühle, K. Kirkpatrick, J. Kremer and D. Andrienko, *Phys. Status Solidi B*, 2008, **245**, 844.

22 V. Marcon, T. Vehoff, J. Kirkpatrick, C. Jeong, D. Yoon, K. Kremer and D. Andrienko, *J. Chem. Phys.*, 2008, **129**, 094505.

23 C. Breneman and K. Wiberg, *J. Comput. Chem.*, 1990, **11**, 361.

24 U. von Barth, *Phys. Scr.*, 2004, **t109**, 9–39.

25 W. L. Jorgensen, D. S. Maxwell and J. Tirado-Rives, *J. Am. Chem. Soc.*, 1996, **118**, 11225.

26 S. Kwasniewski, L. Claes, J.-P. Francois and M. Deleuze, *J. Chem. Phys.*, 2003, **118**, 7823.

27 A. Hoekstra, P. Meertens and A. Vos, *Acta Crystallogr., Sect. B: Struct. Crystallogr. Cryst. Chem.*, 1975, **31**, 2813.

28 K. Zimmerman, *J. Comput. Chem.*, 1991, **12**, 310–319.

29 H. J. C. Berendsen, J. P. M. Postma, A. DiNola and J. R. Haak, *J. Chem. Phys.*, 1984, **81**, 3684.

30 J. P. Ryckaert and A. Bellemans, *Faraday Discuss. Chem. Soc.*, 1978, **66**, 95–106.

31 W. L. Jorgensen and T. B. Nguen, *J. Comput. Chem.*, 1993, **14**, 195–205.

32 W. L. Jorgensen, E. R. Laird, T. B. Nguen and J. Tirado-Rives, *J. Comput. Chem.*, 1993, **14**, 206–215.

33 H. J. Bender and M. D. Zeidler, *Ber. Bunzenges. Phys. Chem.*, 1971, **75**, 236.

34 D. J. Winfield, *J. Chem. Phys.*, 1971, **54**, 3643.

35 C. Collison, L. Rothberg, V. Treemaneekarn and L.Y., *Macromolecules*, 2001, **34**, 2346–2352.

36 M. Knaapila, V. Garamus, L. Dias, F. B. Almasy, F. Galbrecht, A. Charas, J. Morgado, H. Burrows, U. Scherf and A. Monkman, *Macromolecules*, 2006, **39**, 6505–6512.

37 M. Grell, D. Bradley, G. Ungar, J. Hill and K. Whitehead, *Macromolecules*, 1999, **32**, 5810–5817.

38 H.-P. Hsu, W. Paul and K. Binder, *Macromolecules*, 2010, **43**, 3094.

39 L. Schäfer, A. Ostendorf and J. Hager, *J. Phys. A: Math. Gen.*, 1999, **32**, 7875.

40 L. Schäfer and K. Elsner, *Eur. Phys. J. E*, 2004, **13**, 225.

41 L. Siebbeles, F. Grozema, M. de Haas and J. Warman, *Radiat. Phys. Chem.*, 2005, **72**, 85–91.

42 O. A. von Lilienfeld and D. Andrienko, *J. Chem. Phys.*, 2006, **124**, 054307.

43 W. Tschöp, K. Kremer, J. Batoulis, T. Burger and O. Hahn, *Acta Polym.*, 1998, **49**, 61–74.

44 A. Lyubartsev and A. Laaksonen, *Phys. Rev. E: Stat. Phys., Plasmas, Fluids, Relat. Interdiscip. Top.*, 1995, **52**, 3730–3737.

45 S. Izvekov and G. Voth, *J. Chem. Phys.*, 2005, **123**, 134105.

46 W. G. Noid, J. Chu, G. S. Ayton, V. Krishna, S. Izvekov, G. A. Voth, A. Das and H. C. Andersen, *J. Chem. Phys.*, 2008, **128**, 244114.

47 D. Andrienko, S. Leon, L. Delle Site and K. Kremer, *Macromolecules*, 2005, **38**, 5810–5816.

48 X. Zhou, D. Andrienko, L. Delle Site and K. Kremer, *J. Chem. Phys.*, 2005, **123**, 104904.

49 B. Hess, C. Holm and N. van der Vegt, *Phys. Rev. Lett.*, 2006, **96**, 147801.

50 R. Roe, *Methods of X-ray and Neutron Scattering in Polymer Science*, Oxford: New York, 2000.

51 M. Rubinstein and R. Colby, *Polymer Physics*, Oxford: New York, 2003.

52 A. Semenov, *Macromolecules*, 2009, **42**, 6761–6776.

53 D. Hu, J. Yu, K. Wong, B. Bagchi, P. Rossky and P. Barbara, *Nature*, 2000, **405**, 1030.

This journal is © The Royal Society of Chemistry 2010

J. Mater. Chem., 2010, **20**, 10475–10485 | 10485